Realistic indirect spin interactions between magnetic impurities on a metallic Pb(110) surface

Alejandro Rébola [1,*] and Alejandro M. Lobos [2]

[1] *Instituto de Física Rosario-CONICET, Boulevard 27 de Febrero 210 bis, 2000 Rosario, Argentina*

[2] *Instituto Interdisciplinario de Ciencias Básicas, Universidad Nacional de Cuyo, CONICET, Facultad de Ciencias Exactas y Naturales, Padre J. Contreras 1300, (5500) Mendoza, Argentina*

(Received 5 September 2019; published 9 December 2019)

Motivated by recent experiments, here we study the indirect interactions between magnetic impurities deposited on top of a clean Pb(110) surface, induced by the underlying conduction electrons. Our approach makes use of *ab initio* calculations to characterize the clean Pb(110) surface and avoids self-consistency, a feature that greatly reduces the computational cost. In combination with second-order perturbation theory in the microscopic *s-d* exchange parameter J_{sd} between a magnetic adatom and the conduction electrons, we are able to systematically derive the Ruderman-Kittel-Kasuya-Yosida, the Dzyaloshinskii-Moriya, and the anisotropic tensor interactions emerging at the Pb(110) surface between magnetic impurities. The only adjustable parameter is J_{sd}, which is fitted to reproduce the experiments. Our results show important anisotropy effects arising both from the rectangular geometry of the (110) unit cell and from the strong Rashba spin-orbit interaction due to the broken inversion symmetry at the Pb(110) surface. In addition to Pb(110), the characterization of the indirect spin interactions described here could be extended to other realistic metallic surfaces for weakly coupled impurities and would enable us to fabricate atomic-size nanostructures with engineered interactions and on-demand magnetic properties, anticipating useful applications in nanotechnology.

DOI: 10.1103/PhysRevB.100.235412

I. INTRODUCTION

The Rudermann-Kittel-Kasuya-Yosida (RKKY) exchange interaction is an indirect magnetic coupling between localized magnetic moments, mediated by the conduction electrons in a metallic substrate [1–3]. This type of interaction plays a crucial role in systems displaying giant magnetoresistance [4], heavy-fermion magnetism, and quantum criticality [5–7] and in dilute magnetic semiconductors [8,9]. More recently, it has also been observed in atomic-scale magnetic systems fabricated with scanning tunneling microscopy (STM) techniques [10–15] . In these atomic-sized structures the RKKY interaction plays a major role. For instance, it was recently proposed as a key ingredient in magnetic atomic chains deposited on conventional superconductors with a strong Rashba spin-orbit coupling (SOC), systems predicted to host Majorana-fermion quasiparticles (MQPs) [16–18]. These works have triggered a great amount of theoretical and experimental research seeking to observe MQPs, which could be instrumental in the fabrication of qubits for topological quantum computers. In recent experimental works involving atomic Fe chains on top of clean Pb(111) or Pb(110) surfaces, preliminary evidence of MQPs has been reported [19–22].

Assuming an idealized isotropic free-electron conduction band, the standard result for the RKKY interaction is $J_{\mathrm{RKKY}}(\mathbf{r}) \sim \cos(2k_F r)/r^D$, where k_F is the Fermi momentum and $r = |\mathbf{r}|$ is the distance between the magnetic impurities [1–3]. However, the behavior of real adatom systems on metallic surfaces is strikingly different, and departs from an ideally isotropic interaction have been reported experimentally. For instance, one of the most relevant results in Refs. [10–12,15] is the anisotropic character of the RKKY interaction on surfaces. Considering the growing interest in the fabrication of magnetic devices with specific functionalities and potential applications in quantum computing and spintronic and magnetic memories, a detailed characterization of realistic magnetic interactions would be highly desirable. From a more fundamental perspective, a realistic characterization of the RKKY interaction on specific metallic surfaces could also be useful to simulate, in a controlled manner, the physics of strongly correlated materials. For instance, using self-assembled metal-organic networks deposited on clean metallic surfaces, a controlled study of the celebrated Kondo lattice model, typically used to understand the exotic low-temperature behavior of heavy-fermion materials, has become possible with STM techniques [23–25].

Among the many possible metallic surfaces typically studied with STM, the surface of Pb has become an ideal platform to study the interplay between superconductivity and atomic magnetism. The interest is twofold: (1) Pb becomes a conventional *s*-wave superconductor at low temperatures, with a standard phonon-mediated pairing mechanism. In addition, its relative simplicity to grow in films by evaporation techniques makes it a widely used superconducting material in the laboratory. (2) A large Rashba SOC exists at the surface of Pb, a property that is known to induce large Dzyaloshinskii-Moriya interactions. This property could be exploited in order to engineer noncollinear chiral magnetic nanostructures, such as skyrmions [14,26]. Both features could prove extremely useful in novel spintronic devices [27–31]. In previous works, perturbative approaches

*rebola@ifir-conicet.gov.ar

combined with numerical and/or semianalytical methods for realistic band-structure calculations were used for the calculation of the RKKY indirect-exchange interaction between nuclear moments [32–35]. However, none of these works have focused on magnetic impurities on Pb, where relativistic effects are unavoidable. On the other hand, the calculation of the Dzyaloshinskii-Moriya interaction was tackled in previous works using highly idealized model Hamiltonians [26,36–38], which ignore the real electronic structure. Therefore, there are no systematic studies of the realistic magnetic interactions on the surface of Pb.

Motivated by the aforementioned experimental advances, in this paper we focus on the derivation of realistic magnetic interactions between impurities on top of a clean Pb surface. For concreteness and in order to make a comparison with Refs. [19–22], we have chosen the particular case of Pb(110). However, we stress that our method is not restricted to any specific system. Using a combination of an analytical approach, i.e., second-order perturbation theory in the *s-d* exchange interaction J_{sd}, and density functional theory (DFT) to obtain the full band structure of Pb(110), including relativistic SOC effects, we systematically derive the RKKY, the Dzyaloshinskii-Moriya (DM), and the anisotropic tensor interactions between magnetic impurities. Our results show important anisotropy effects arising both from the rectangular geometry of the (110) unit cell and from the strong Rashba SOC originating in the broken inversion symmetry at the Pb(110) surface. Since within our perturbative approach only the band structure of the *clean* Pb(110) surface is needed, the computational cost can be significatively reduced. This represents one of the main advantages of our method: The possibility to describe indirect magnetic interactions realistically (i.e., without having to resort to any *a priori* model or approximation), combined with low computational cost compared to standard self-consistent methods, such as the Korringa-Kohn-Rostoker method. Within our formalism, the only adjustable parameter is the *s-d* exchange parameter J_{sd}, which is fitted to reproduce experiments [39].

Like any perturbative approach, the method outlined in this work relies on the impurities being weakly coupled to the metallic surface. More explicitly, it is required that $\rho_{3D}J_{sd} \ll 1$, where ρ_{3D} is the density of conduction states per unit volume at the Fermi level. This fact, however, does not constitute a major drawback for its applicability since many of the interesting systems realized in experiments fall within the weak-coupling regime. This is the case of metal-organic complexes such as MnPc molecules [39] and iron II porphyrin molecules [40] deposited on top of Pb(110), where the organic ligand of the molecule tends to isolate the effective magnetic moment from the surface, leading to a small effective coupling J_{sd}, and organic molecules of the nitronyl nitroxide side group adsorbed on an Au(111) surface [41].

The rest of the paper is organized as follows. In Sec. II we present the theoretical model and the derivation of the generic RKKY, DM, and tensor interactions directly from the conduction-electron propagators. In Sec. III we give details about the technical aspects of the *ab initio* calculations and about the convergence of the RKKY interaction. In Sec. IV we present the results; specifically, in Sec. IV A we present our results for the band structure of the clean Pb(110), and in Sec. IV C we show our results for the magnetic RKKY, DM, and tensor interactions. Finally, in Sec. V we summarize the main results and present the conclusions.

II. THEORETICAL MODEL AND DERIVATION OF THE EFFECTIVE INTERACTIONS

The theoretical model describing two spin impurities on a Pb(110) surface, located at sites $\mathbf{r}_1 = (x_1, y_1, 0)$ and $\mathbf{r}_2 = (x_2, y_2, 0)$, where $z = 0$ is the coordinate of the surface plane, is

$$H = H_0 + H_{sd}(1) + H_{sd}(2). \tag{1}$$

Here

$$H_0 = \sum_{\mathbf{k},n} \epsilon^{(0)}_{\mathbf{k},n} c^\dagger_{\mathbf{k},n} c_{\mathbf{k},n} \tag{2}$$

is the unperturbed Hamiltonian describing the bands of clean Pb(110). The quantum numbers $\mathbf{k}$ and n are, respectively, the crystal momentum parallel to the surface belonging to the first Brillouin zone and the spin-orbital band index, which results from a combination of the spin and the azimuthal angular momentum (recall that in the presence of Rashba and/or Dresselhaus SOC, s, the spin projection along z, is no longer a good quantum number. In the absence of Rashba SOC, the index n splits into s and the usual band index α). The operator $c_{\mathbf{k},n}$ annihilates a fermionic quasiparticle in the conduction band and obeys the usual anticommutation relation $\{c_{\mathbf{k},n}, c^\dagger_{\mathbf{k}',n'}\} = \delta_{\mathbf{k},\mathbf{k}'}\delta_{n,n'}$. Finally, $\epsilon^{(0)}_{\mathbf{k},n}$ is the dispersion relation computed in the absence of the magnetic impurities.

The *s-d* exchange interaction between a magnetic moment and the conduction-electron spin density at point $\mathbf{r}_j$ is [6]

$$H_{sd}(j) = J_{sd}\mathbf{S}_j \cdot \mathbf{s}(\mathbf{r}_j) \tag{3}$$

$$= J_{sd}\mathbf{S}_j \cdot \sum_{s,s'=\{\uparrow,\downarrow\}} \Psi^\dagger_s(\mathbf{r}_j) \left(\frac{\hat{\boldsymbol{\sigma}}}{2}\right)_{ss'} \Psi_{s'}(\mathbf{r}_j), \tag{4}$$

where $\mathbf{S}_j$ is the spin of the impurity, which is assumed to be a classical quantity, and where $\hat{\boldsymbol{\sigma}} = (\hat{\sigma}_x, \hat{\sigma}_y, \hat{\sigma}_z)$ is the vector of Pauli matrices. The field operator

$$\Psi_s(\mathbf{r}_j) = \sum_{\mathbf{k},n} \psi^{(s)}_{\mathbf{k},n}(\mathbf{r}_j) c_{\mathbf{k},n} \tag{5}$$

annihilates a fermionic quasiparticle with spin projection $s = \{\uparrow,\downarrow\}$ along the z axis at point $\mathbf{r}_j$, and $\psi^{(s)}_{\mathbf{k},n}(\mathbf{r})$ are the normalized Bloch wave functions computed via DFT (see Sec. III). The field operator obeys the usual relations:

$$\sum_{\mathbf{k},n} \psi^{*(s)}_{\mathbf{k},n}(\mathbf{r}_i)\, \psi^{(s')}_{\mathbf{k},n}(\mathbf{r}_j) = \delta(\mathbf{r}_i - \mathbf{r}_j)\delta_{s,s'}, \tag{6}$$

$$\{\Psi_s(\mathbf{r}_i), \Psi^\dagger_{s'}(\mathbf{r}_j)\} = \delta(\mathbf{r}_i - \mathbf{r}_j)\delta_{s,s'}. \tag{7}$$

The idea now is to use knowledge of the *realistic* band structure of Pb(110), encoded in $\epsilon^{(0)}_{\mathbf{k},n}$ and $\psi^{(s)}_{\mathbf{k},n}(\mathbf{r}_j)$, in order to systematically derive all the effective interactions between $\mathbf{S}_1$ and $\mathbf{S}_2$ mediated by the conduction electrons using second-order perturbation theory in J_{sd} and without resorting to any specific model. In the process, not only is the RKKY exchange obtained, but so are Dzyaloshinskii-Moriya and anisotropic tensor interactions.

We start from the full partition function of the system, which is formally written as

$$Z = \mathrm{Tr}\left\{e^{-\beta(H_0+\sum_j H_{sd}(j))}\right\}, \\ = \mathrm{Tr}_S\,\mathrm{Tr}_\psi\left\{e^{-\beta(H_0+\sum_j H_{sd}(j))}\right\}, \quad (8)$$

where $\beta = 1/T$ (here we have assumed $k_B = 1$). In Eq. (8) we have split the total trace into partial traces over fermionic (denoted Tr_ψ) and spin (denoted Tr_S) degrees of freedom. This allows us to define the quantity $Z_S \equiv \mathrm{Tr}_\psi\{e^{-\beta[H_0+\sum_j H_K(j)]}\}$, where the partial trace over the electrons is taken considering a particular "frozen" configuration of the spins $\mathbf{S}_1$ and $\mathbf{S}_2$. In the zero-temperature limit $\beta \to \infty$, this quantity allows us to define an effective spin Hamiltonian where the electronic degrees of freedom have been integrated out,

$$Z_S = Z_0 e^{-\beta H_{\mathrm{eff}}[\mathbf{S}_1,\mathbf{S}_2]} \ (\beta \to \infty). \quad (9)$$

Using the path-integral formalism [42], Z_S can be expressed as

$$Z_S = \int \mathcal{D}[\bar{c}, c]\ e^{-\mathcal{S}_0[\bar{c},c]-\sum_j \mathcal{S}_{sd,j}[\mathbf{S}_j,\bar{c},c]},$$

where $\bar{c}, c$ are Grassmann variables and $\mathcal{S}_0[\bar{c}, c]$ and $\mathcal{S}_{sd,j}[\mathbf{S}_j, \bar{c}, c]$ are, respectively,

$$\mathcal{S}_0[\bar{c}, c] = \sum_{\mathbf{k},n}\int_0^\beta d\tau\ \bar{c}_{\mathbf{k},n}(\tau)\left(\partial_\tau - \epsilon^{(0)}_{\mathbf{k},n}\right)c_{\mathbf{k},n}(\tau), \quad (10)$$

the Euclidean action of the unperturbed Pb(110), expressed as an integral over Matsubara time τ in the interval $[0, \beta]$, and

$$\mathcal{S}_{sd,j}[\mathbf{S}_j, \bar{c}, c] = J_{sd}\mathbf{S}_j \sum_{s,s'}\int_0^\beta d\tau\, \Psi^\dagger_s(\mathbf{r}_j, \tau)\frac{\hat{\boldsymbol{\sigma}}_{ss'}}{2}\Psi_{s'}(\mathbf{r}_j, \tau), \quad (11)$$

the Euclidean action of the s-d interaction. The advantage of the path-integral formalism is that it allows us to express Z_S as a series expansion in powers of J_{sd} as

$$Z_S = Z_0\sum_{m=0}^\infty \frac{1}{m!}\left\langle\left(\sum_j \mathcal{S}_{sd,j}[\mathbf{S}_j, \bar{c}, c]\right)^m\right\rangle_0, \quad (12)$$

where the notation $\langle A\rangle_0$ means the average of operator A with respect to the action $\mathcal{S}_0$, i.e., $\langle A\rangle_0 = \int \mathcal{D}[\bar{c}, c]\ e^{-\mathcal{S}_0[\bar{c},c]}A_0/Z_0$, with $Z_0 = \int \mathcal{D}[\bar{c}, c]\ e^{-\mathcal{S}_0[\bar{c},c]}$ being the partition function of unperturbed electrons in Pb(110).

Equations (8)–(12) are formally exact, but in order to make progress we need to introduce a truncation in the infinite series in Eq. (12), assuming $J_{sd} \to 0$. At second order, and introducing a subsequent cumultant expansion [43], the quantity Z_S can be approximated as

$$Z_S \approx Z_0 e^{\frac{1}{2}\langle(\mathcal{S}_{sd,1}[\mathbf{S}_1,\bar{c},c]+\mathcal{S}_{sd,2}[\mathbf{S}_2,\bar{c},c])^2\rangle_0} \quad (13)$$

[note that the first-order term in (12) has vanished due to the time-reversal symmetry of the Pb(110) conduction band]. Comparing Eqs. (9) and (13), we obtain the precise analytical form for the effective spin Hamiltonian at second order in J_{sd}:

$$H_{\mathrm{eff}} = \lim_{\beta\to\infty} -\frac{1}{2\beta}\langle(S_{sd,1}[\mathbf{S}_1, \bar{c}, c] + S_{sd,2}[\mathbf{S}_2, \bar{c}, c])^2\rangle_0, \quad (14)$$

where the conduction electrons of the Pb(110) band have been integrated out. The effective Hamiltonian can be expressed as

$$H_{\mathrm{eff}} = \lim_{\beta\to\infty}\frac{J_{sd}^2}{8}\frac{1}{\beta}\sum_l\sum_{i,j=1,2} \\ \times \mathrm{tr}\{(\mathbf{S}_i.\hat{\boldsymbol{\sigma}})\hat{\mathbf{g}}_0(\mathbf{r}_i, \mathbf{r}_j, i\nu_l)(\mathbf{S}_j.\hat{\boldsymbol{\sigma}})\hat{\mathbf{g}}_0(\mathbf{r}_j, \mathbf{r}_i, i\nu_l)\}, \quad (15)$$

where $\mathrm{tr}\{\cdots\}$ is the usual trace of a matrix and $\hat{\mathbf{g}}_0\left(\mathbf{r}_i, \mathbf{r}_j, i\nu_l\right)$ is the matrix of the unperturbed conduction-electron propagators in Pb(110),

$$\hat{\mathbf{g}}_0(\mathbf{r}_i, \mathbf{r}_j, i\nu_l) = \begin{pmatrix} g_0^{(\uparrow\uparrow)}(\mathbf{r}_j, \mathbf{r}_i, i\nu_l) & g_0^{(\uparrow\downarrow)}(\mathbf{r}_j, \mathbf{r}_i, i\nu_l) \\ g_0^{(\downarrow\uparrow)}(\mathbf{r}_j, \mathbf{r}_i, i\nu_l) & g_0^{(\downarrow\downarrow)}(\mathbf{r}_j, \mathbf{r}_i, i\nu_l)\end{pmatrix}, \quad (16)$$

with matrix elements

$$g_0^{(ss')}(\mathbf{r}_j, \mathbf{r}_i, i\nu_l) = \sum_{\mathbf{k},n}\frac{\psi^{(s)}_{\mathbf{k}n}(\mathbf{r}_j)\psi^{*(s')}_{\mathbf{k}n}(\mathbf{r}_i)}{i\nu_l - \epsilon^{(0)}_{\mathbf{k},n}}\ (s, s' = \{\uparrow, \downarrow\}). \quad (17)$$

In this expression we have introduced the fermionic Matsubara frequencies $i\nu_l = 2\pi i\left(l + \frac{1}{2}\right)/\beta$. Physically, the Green's function $g_0^{(ss')}\left(\mathbf{r}_j, \mathbf{r}_i, i\nu_l\right)$ measures the probability that an electron created at $\mathbf{r}_i$ with spin s' arrives at $\mathbf{r}_j$ with spin s in the unperturbed surface of Pb(110). Note that in the absence of SOC, the spin-projection labels s and s' would be good quantum numbers, and therefore, the off-diagonal elements would vanish. Moreover, due to the SU(2) symmetry in the absence of SOC and externally applied magnetic fields, $g_0^{(\uparrow\uparrow)}\left(\mathbf{r}_j, \mathbf{r}_i, i\nu_l\right) = g_0^{(\downarrow\downarrow)}\left(\mathbf{r}_j, \mathbf{r}_i, i\nu_l\right)$, and therefore, the matrix $\hat{\mathbf{g}}_0\left(\mathbf{r}_i, \mathbf{r}_j, i\nu_l\right)$ would be a scalar proportional to the unit matrix. In what follows, we introduce a more convenient representation of the propagator matrix (16) in terms of the 2×2 Pauli matrices [44],

$$\hat{\mathbf{g}}_0(\mathbf{r}_i, \mathbf{r}_j, i\nu_l) = g_0^0(\mathbf{r}_i, \mathbf{r}_j, i\nu_l)\mathbf{1}_{2\times 2} + g_0^x(\mathbf{r}_i, \mathbf{r}_j, i\nu_l)\hat{\sigma}_x \\ + g_0^y(\mathbf{r}_i, \mathbf{r}_j, i\nu_l)\hat{\sigma}_y + g_0^z(\mathbf{r}_i, \mathbf{r}_j, i\nu_l)\hat{\sigma}_z, \quad (18)$$

where the new propagators $g_0^k\left(\mathbf{r}_i, \mathbf{r}_j, i\nu_l\right)$ (with $k = \{0, x, y, z\}$) are linear combinations of the propagators (17), which allow us to readily evaluate the trace in Eq. (15) and express the Hamiltonian as

$$H_{\mathrm{eff}}[\mathbf{S}_1, \mathbf{S}_2] = J_{\mathrm{RKKY}}(\mathbf{r}_1, \mathbf{r}_2)\,\mathbf{S}_1\cdot\mathbf{S}_2 + \mathbf{D}_{\mathrm{DM}}(\mathbf{r}_1, \mathbf{r}_2)\cdot(\mathbf{S}_1\times\mathbf{S}_2) \\ + 2\mathbf{S}_1\cdot\mathbf{T}(\mathbf{r}_1, \mathbf{r}_2)\cdot\mathbf{S}_2 + \mathbf{S}_1\cdot\mathbf{T}(\mathbf{r}_1, \mathbf{r}_1)\cdot\mathbf{S}_1 \\ + \mathbf{S}_2\cdot\mathbf{T}(\mathbf{r}_2, \mathbf{r}_2)\cdot\mathbf{S}_2. \quad (19)$$

Here we have defined the scalar RKKY exchange interaction as

$$J_{\mathrm{RKKY}}(\mathbf{r}_1, \mathbf{r}_2) = \frac{J_{sd}^2}{2}\frac{1}{\beta}\sum_l\Big[g_0^0(\mathbf{r}_1, \mathbf{r}_2, i\nu_l)\,g_0^0(\mathbf{r}_2, \mathbf{r}_1, i\nu_l) \\ - \sum_{j=\{x,y,z\}} g_0^j(\mathbf{r}_1, \mathbf{r}_2, i\nu_l)\,g_0^j(\mathbf{r}_2, \mathbf{r}_1, i\nu_l)\Big]. \quad (20)$$

The next term in Eq. (19) corresponds to the Dzyaloshinskii-Moriya interaction

$$D^{j}_{\mathrm{DM}}(\mathbf{r}_1,\mathbf{r}_2) = i\frac{J^2_{sd}}{2}\frac{1}{\beta}\sum_{l}\left[g^0_0(\mathbf{r}_1,\mathbf{r}_2,i\nu_l)\,g^j_0(\mathbf{r}_2,\mathbf{r}_1,i\nu_l) - g^j_0(\mathbf{r}_1,\mathbf{r}_2,i\nu_l)\,g^0_0(\mathbf{r}_2,\mathbf{r}_1,i\nu_l)\right] \times (j=\{x,y,z\}), \tag{21}$$

which is an anisotropic vector interaction. Finally, the last terms are anisotropic tensor interactions of the form

$$T^{jk}(\mathbf{r}_1,\mathbf{r}_2) = \frac{J^2_{sd}}{4}\frac{1}{\beta}\sum_{l}\left[g^j_0(\mathbf{r}_1,\mathbf{r}_2,i\nu_l)\,g^k_0(\mathbf{r}_2,\mathbf{r}_1,i\nu_l) + g^j_0(\mathbf{r}_2,\mathbf{r}_1,i\nu_l)\,g^k_0(\mathbf{r}_1,\mathbf{r}_2,i\nu_l)\right] \times (j,k=\{x,y,z\}), \tag{22}$$

which generalize the Ising and the single-ion magnetocrystalline contributions. Note that in (19) we have neglected the RKKY self-interaction terms $J_{\mathrm{RKKY}}(\mathbf{r}_j,\mathbf{r}_j)\mathbf{S}^2_j$ since they are only a renormalization of the energy.

Although the three contributions (20)–(22) are of the same order, $O\left(J^2_{sd}\right)$, their relative magnitude strongly depends on the magnitude of the Rashba SOC parameter α_R. This can be understood directly at the level of the propagators $g^{(x,y)}_0(\mathbf{r}_1,\mathbf{r}_2,i\nu_l)$ appearing in these expressions, which are directly proportional to the SU(2) symmetry-breaking terms in the Hamiltonian, as shown in previous works [26,44]. Then, it is easy to see that

$$J_{\mathrm{RKKY}}(\mathbf{r}_1,\mathbf{r}_2)\sim O(1),$$
$$|\mathbf{D}_{\mathrm{DM}}(\mathbf{r}_1,\mathbf{r}_2)|\sim O(\alpha_R),$$
$$\|\mathbf{T}(\mathbf{r}_1,\mathbf{r}_2)\|\sim O\left(\alpha^2_R\right).$$

III. METHODS AND TECHNICAL CONSIDERATIONS

A technical point in the derivation of the RKKY interaction (20) concerns the sum over the band index n, whose convergence is very slow. In principle, this sum runs over an infinite number of bands but in practice must be limited by a cutoff energy E_c that ensures the convergence of the involved quantities. Due to its poor convergence properties, for a reasonable accuracy in the value of $J_{\mathrm{RKKY}}(\mathbf{r}_1,\mathbf{r}_2)$ an unfeasibly large value of E_c would be necessary (even for values of the order of $E_c = 100$ eV, errors would still be over 100%). However, it is physically expected that above a certain E_c the system wave functions are indistinguishable from the corresponding free-electron wave functions at the same energy. In other words, at sufficiently high energies $\epsilon^{(0)}_{\mathbf{k},n}$, it is expected that

$$\epsilon^{(0)}_{\mathbf{k},n}\approx\epsilon^{\mathrm{free}}_{\mathbf{k}}=\frac{\hbar^2(\mathbf{k}+\mathbf{G}_n)^2}{2m}, \tag{23}$$

$$\psi^{(s)}_{\mathbf{k}n}(\mathbf{r})\approx\frac{e^{i(\mathbf{k}+\mathbf{G}_n)\cdot\mathbf{r}}}{\sqrt{V}}, \tag{24}$$

with $\mathbf{G}_n$ being a reciprocal-lattice vector. Taking this into account, the RKKY exchange interaction (20) at $T=0$ can then be recast as

$$J_{\mathrm{RKKY}}(\mathbf{r}_1,\mathbf{r}_2) = J^0_{\mathrm{RKKY}}(\mathbf{r}_1,\mathbf{r}_2) + J^{\mathrm{free}}_{\mathrm{RKKY}}(\mathbf{r}_1,\mathbf{r}_2), \tag{25}$$

where

$$J^0_{\mathrm{RKKY}}(\mathbf{r}_1,\mathbf{r}_2) = \frac{J^2_{sd}}{4}\sum_{s=\{\uparrow,\downarrow\}}\sum_{\mathbf{k},n}^{\epsilon_{\mathbf{k}n}<E_F}\frac{1}{V}\sum_{\mathbf{k}',n'}^{E_F<\epsilon_{\mathbf{k}'n'}<E_c}\frac{1}{\epsilon^{(0)}_{\mathbf{k}n}-\epsilon^{(0)}_{\mathbf{k}'n'}} \times\left[\psi^{(s)}_{\mathbf{k}n}(\mathbf{r}_1)\,\psi^{*(s)}_{\mathbf{k}n}(\mathbf{r}_2)\,\psi^{(\bar{s})}_{\mathbf{k}'n'}(\mathbf{r}_2)\,\psi^{*(\bar{s})}_{\mathbf{k}'n'}(\mathbf{r}_1) - \psi^{(s)}_{\mathbf{k}n}(\mathbf{r}_1)\,\psi^{*(\bar{s})}_{\mathbf{k}n}(\mathbf{r}_2)\,\psi^{(\bar{s})}_{\mathbf{k}'n'}(\mathbf{r}_2)\,\psi^{*(s)}_{\mathbf{k}'n'}(\mathbf{r}_1)\right], \tag{26}$$

$$J^{\mathrm{free}}_{\mathrm{RKKY}}(\mathbf{r}_1,\mathbf{r}_2) = \frac{J^2_{sd}}{4}\sum_{s=\{\uparrow,\downarrow\}}\sum_{\mathbf{k},n}^{\epsilon_{\mathbf{k}n}<E_F}\frac{1}{V}\sum_{\mathbf{k}'}^{E_c<\epsilon_{\mathbf{k}'}}\left[\psi^{(s)}_{\mathbf{k}n}(\mathbf{r}_1)\,\psi^{*(s)}_{\mathbf{k}n}(\mathbf{r}_2) - \psi^{(s)}_{\mathbf{k}n}(\mathbf{r}_1)\,\psi^{*(\bar{s})}_{\mathbf{k}n}(\mathbf{r}_2)\right]\frac{e^{i\mathbf{k}'\cdot(\mathbf{r}_2-\mathbf{r}_1)}}{\epsilon^{(0)}_{\mathbf{k}n}-\epsilon^{\mathrm{free}}_{\mathbf{k}'}}, \tag{27}$$

where in this last equation we have dropped the index n' and let $\mathbf{k}'$ run over the extended Brillouin zone. $J^{\mathrm{free}}_{\mathrm{RKKY}}(\mathbf{r}_1,\mathbf{r}_2)$ is then a free-electron correction term that can be analytically integrated and that only depends on states below the Fermi energy and on the numerical value of E_c. In this way, instead of summing over a large number of bands, Eq. (25) needs to be evaluated only until convergence with respect to E_c is attained.

The wave functions $\psi^{(s)}_{\mathbf{k},n}(\mathbf{r}_j)$ required to calculate the interactions (20)–(22) for both impurities were obtained from DFT calculations performed by using the VASP code [45–47]. The Pb(110) substrate was modeled as a periodic slab consisting of a 1×1 surface with N layers of Pb atoms and a vacuum layer of 15 Å to avoid coupling between surfaces in different periodic cells. Three top layers were allowed to relax while the other ones where kept fixed at their bulk lattice coordinates. Ionic forces were converged to be lower than 0.01 eV/Å, with a cutoff of 150 eV and using a Monhorst-Pack [48] grid of $10\times10\times1$ k points. All calculations were performed within the projector augmented wave method [49] and using Perdew-Burke-Ernzerhof revised for solids exchange-correlation functional [50]. Since the interactions (20)–(22) are highly dependent on the accuracy of the wave functions $\psi^{(s)}_{\mathbf{k},n}(\mathbf{r}_j)$, a more stringent convergence condition and a larger number of empty bands were needed in their calculation. In order to obtain errors within 5% we used 120 empty bands and 1600 k points. Calculations were performed with and without atomic spin-orbit interaction.

IV. RESULTS

A. Band structure of Pb(110) and estimation of Rashba coupling parameter

The band structure of Pb(110) bulk and surface was first studied by Würde *et al.* [51] using the empirical tight-binding method (ETBM) combined with the scattering-theory method to determine the different surface and resonant states. Given the large atomic number of Pb, the effect of the spin-orbit interaction cannot be neglected for this system and needs to be taken into account. In the present work the Pb(110) band structure was obtained by self-consistent DFT calculations by including spin-orbit coupling and by also considering relaxation effects on the (110) surface. In Fig. 1 we show the calculated band structure for a Pb(110) slab with $N=29$ layers. The surface and resonant states (red dots) are identified

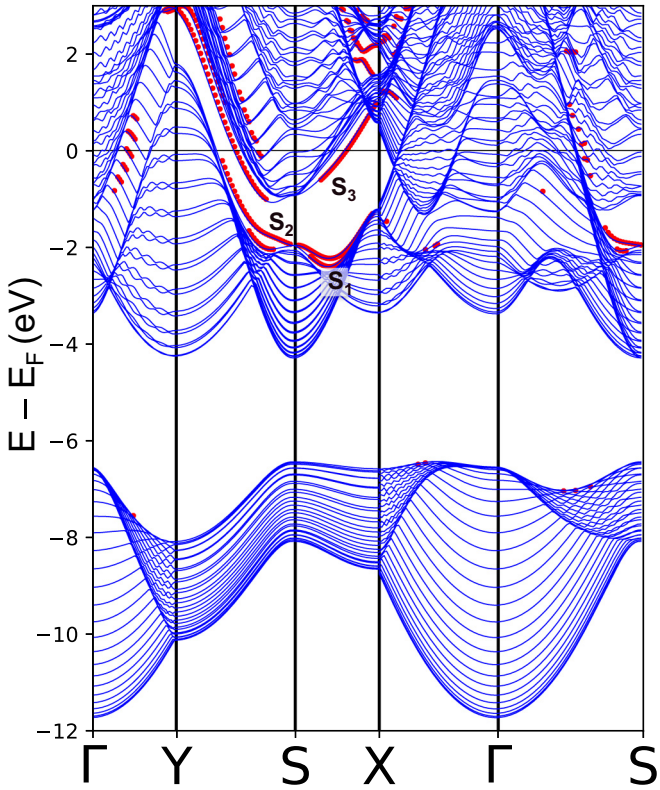

FIG. 1. Calculated band structure for a 29-layer Pb(110) slab along high-symmetry paths of the Brillouin zone. Surface and resonant states, represented by red dots, have been obtained by requiring the density for a given state projected onto the surface layers (top and bottom) be greater than 0.3. The surface states are labeled S_1, S_2, and S_3.

as those for which the sum of the square projections onto the top and bottom layers of the slab is greater than 30%. These results are in excellent agreement with the ETBM calculations of Würde *et al.* The large gap in the range between −6.5 and −4 eV corresponds to the marked energy difference between *s* and *p* levels in bulk Pb. Surface states (denoted as S_1, S_2, and S_3 in Fig. 1) are mainly localized near the edges of the gaps arising along the *X* and *Y* directions and extend between −2.4 and 3 eV. Bands S_1 and S_2 (S_3) consist mostly of *p* states parallel (perpendicular) to the 110 surface. While the gap opening at point S for $E = -2$ eV is a consequence of spin-orbit coupling, the splitting of bands S_1 and S_2 arises from the Rashba shift at S, generated by the breaking of the symmetry along *z*. Indeed, by using the $\mathbf{k}\cdot\mathbf{p}$ approximation to fit bands S_1 and S_2, it is possible to estimate the Rashba parameter to be $\alpha_R = 0.97$ eV Å.

The excellent agreement with the results by Würde *et al.* justifies the use of the Kohn-Sham orbitals as the wave functions $\psi^{(s)}_{\mathbf{k}n}(\mathbf{r}_j)$ appearing in the expression of the unperturbed propagator Eq. (17) and in the calculation of the magnetic interactions (20)–(22).

B. Convergence of the RKKY interaction

In order to ensure the convergence of the RKKY interaction with respect to the cutoff E_c, we evaluated the function $J_{\mathrm{RKKY}}(\mathbf{r}_1, \mathbf{r}_2)$ as in Eq. (25). Since the magnitude of the correction term $J^{\mathrm{free}}_{\mathrm{RKKY}}(\mathbf{r}_1, \mathbf{r}_2)$ varies inversely with the distance between the two impurities, impurities located at larger distances would require smaller values of E_c in order to converge. For this reason the cutoff energy needs to be optimized for the minimum distance considered, which in our case corresponds to one half of the *b* lattice parameter (or, in other words, when $|\mathbf{r_2} - \mathbf{r_1}| = 0.5b$). In Fig. 2 we display the total coupling $J_{\mathrm{RKKY}} \equiv J_{\mathrm{RKKY}}(0, 0.5b\,\hat{\mathbf{y}})$ together with $J^0 \equiv J^0_{\mathrm{RKKY}}(0, 0.5b\,\hat{\mathbf{y}})$ and its correction $J^{\mathrm{free}} \equiv J^{\mathrm{free}}_{\mathrm{RKKY}}(0, 0.5b\,\hat{\mathbf{y}})$, corresponding to a Pb(110) slab with $N = 11$ Pb layers for different values of the cutoff energy E_c, taken with respect to E_F. Two observations become apparent in the plot. On the one hand, we have the slowly decreasing rate of the correction terms (actually, oscillatory and analogous to the integral sine and cosine functions), which makes them impossible to neglect even for a very high energy cutoff. On the other hand, we observe that the correction closely compensates the variation of J^0 with respect to the cutoff. Despite the fact that for small values of E_c the free-electron approximation is still too crude and the errors are large, for values of E_c larger than $E_F + 20$ eV, the rate of variation of J^{free} clearly mirrors J^0. In this last case, the total J_{RKKY} becomes flat and converges within 2% of the error. The same calculations were repeated for a $N = 17$ layer slab, leading to a similar cutoff and the same values for J_{RKKY} (always within 2% error) as for the 11-layer case. In the light of these results and for the sake of simplicity, the rest of our calculations were performed for an 11-layer slab using the value $E_c = E_F + 22$ eV.

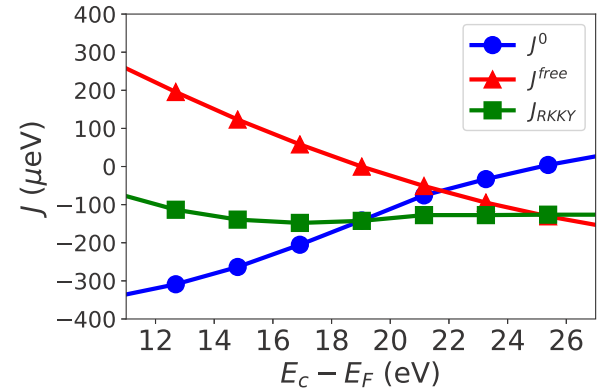

FIG. 2. Convergence of the RKKY interaction J_{RKKY} (green squares) computed as in Eq. (25) as a function of the plane-wave cutoff energy $E_c - E_F$. Convergence is attained when the free-electron correction J^{free} (red triangles) exactly mirrors the uncorrected RKKY term J^0 (blue circles) for $E_c = 22$ eV above E_F.

C. Magnetic interactions

As mentioned in the Introduction, the free parameter J_{sd} must be determined to provide the correct energy scale of the magnetic interactions in Eqs. (20)–(22). The effective coupling $\rho_{3\mathrm{D}}J_{sd}$ can be reliably extracted from experiments [39,41] using the third-order Anderson-Appelbaum perturbative approach [52–54]. From the aforementioned experiments, typical values of $\rho_{3\mathrm{D}}J_{sd}$ between 0.04 and 0.12 were obtained for magnetic impurities in the weak-coupling limit. In what

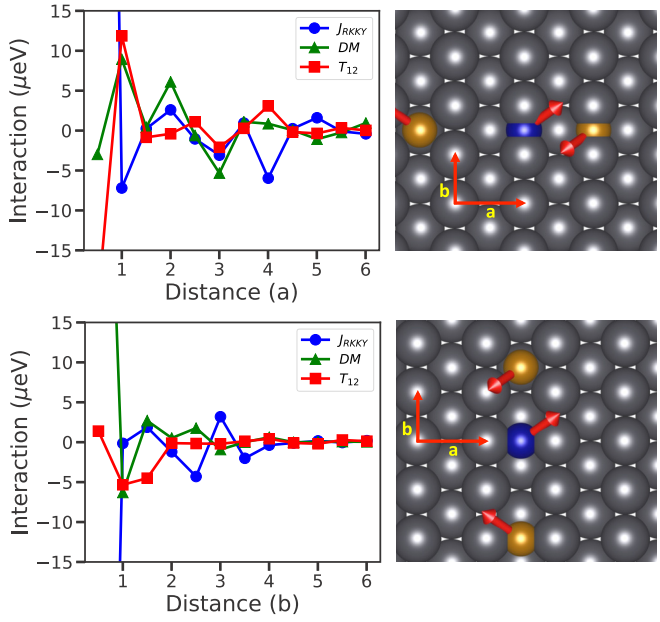

FIG. 3. Top (Bottom): RKKY, DM, and T_{12} magnetic interaction parameters for configurations with the reference impurity (blue) placed at the middle of the shorter (longer) bridge between two Pb atoms on the (110) surface and the second impurity (yellow) placed at $na/2$ ($nb/2$) lattice parameters away along the a (b) direction.

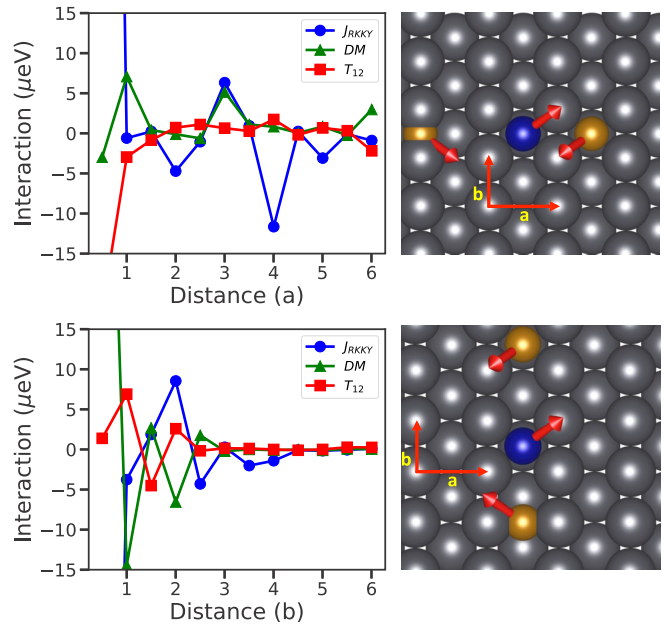

FIG. 4. Top (Bottom): RKKY, DM, and T_{12} magnetic interaction parameters for configurations with the reference impurity (blue) placed at $(0.5a, 0.5b)$ on the (110) surface and the second impurity (yellow) placed at $na/2$ ($nb/2$) lattice parameters away along the a (b) direction.

follows, we illustrate our results using $\rho_{3D}J_{sd} = 0.1$, which falls within the experimentally relevant regime. We then use DFT to calculate ρ_{3D} [i.e., the density of states at the Fermi level for Pb located on the (110) surface] to obtain $J_{sd} = 10.80\,\text{eV}\,\text{Å}^3$.

Once the parameter J_{sd} is determined, the different magnetic interactions in Eqs. (20)–(22) are calculated as a function of distance for impurities located along the a and b directions on the Pb(110) surface. We considered two inequivalent positions for each impurity at the surface, locating it either halfway on the bridge between two Pb atoms of the top layer or above a Pb atom belonging to the layer immediately below [i.e., at $(0.5a, 0.5b)$]. In Fig. 3 we plot the RKKY, DM, and anisotropic-tensor (T_{12}) interactions locating a reference impurity at the bridge between two Pb atoms and letting the second impurity be located at either inequivalent position in such a way that the distance between impurities is either an integer or half integer of one of the in-plane lattice parameters. The top and bottom panels in Fig. 3 display the calculated interactions for the reference impurity at a bridge location and the second impurity at different distances along the a and b directions, respectively. In Fig. 4 we repeated the calculations but this time locating the reference magnetic impurity at $(0.5a, 0.5b)$. In spite of the fact that all interactions follow the expected oscillatory behavior, their character departs significantly from the smooth and monotonic decay of the classical RKKY. It is also worth noticing the anisotropic character of the interactions: While we still encounter large peaks for impurities located four lattice parameters apart along a, interactions are significantly reduced for the same relative distance along b. This behavior, which at first glance may seem counterintuitive (since the impurities are at a closer distance along b), can be qualitatively understood by noticing that the flatter bands along a give rise to a larger density of states along this direction than along b, thus enhancing the magnitude of the interactions.

With the calculated magnetic interactions (J_{RKKY}, DM, T_{12}) it is then possible to search the spin configurations that minimize the effective Hamiltonian (19); that is, we can obtain the classical ground-state configuration. In the top and bottom panels of Fig. 5, we display these configurations together with their corresponding energies for interacting spins located at $\mathbf{r}_1 = (0.5a, 0.5b, 0)$ and $\mathbf{r}_2 = ((0.5 + n)a, 0.5b, 0)$ and at $\mathbf{r}_1 = (0.5a, 0.5b, 0)$ and $\mathbf{r}_1 = (0.5a, (0.5 + nb), 0)$, respectively. Taking, for instance, impurities one lattice parameter apart along the a direction, we see from Fig. 4 that in this case the dominant interaction is DM, thus favoring a canted spin configuration, like the one shown in Fig. 5. Analogously, when the impurities are located two lattice parameters apart along the a direction, both DM and T_{12} interactions nearly vanish, and the dominant interaction is RKKY, resulting in a collinear spin configuration, which, since $J_{\text{RKKY}} < 0$, is ferromagnetic. Along the b direction, the behavior of magnetic ground-state energy is approximately monotonic, and its value is abruptly reduced after $n = 3b$ and beyond. Contrarily, along the a direction the overall behavior is clearly not monotonic, and the magnetic energy gain has a minimum at a distance $n = 4a$. This is a clear deviation from the RKKY interaction mediated by an idealized parabolic band.

Finally, we note that the orders of magnitude of the interactions in Figs. 3, 4, and 5 are in agreement with recent experimental works on Fe atoms deposited on top of Pt(111) [14].

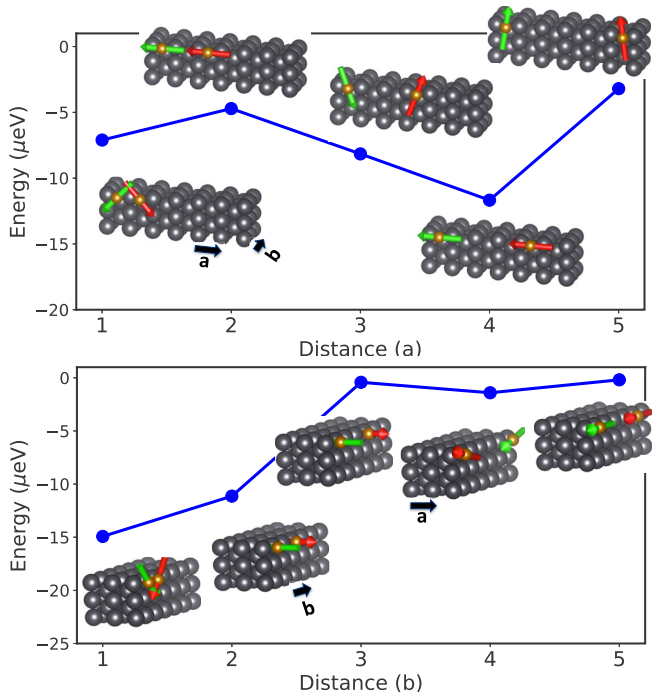

FIG. 5. Top: Ground-state energies and their corresponding spin configurations for the magnetic Hamiltonian of Eq. (15) with a reference impurity (blue) located at $(0.5a, 0.5b)$ interacting with impurities (yellow) located at $(0.5na, 0.5b)$ on the Pb (110) surface. Bottom: Now the impurities interact along the **b** direction; that is, the second impurity is placed at $(0.5a, 0.5nb)$.

V. SUMMARY AND CONCLUSIONS

We have investigated the indirect spin-spin interactions at the (110) surface of Pb, mediated by conduction electrons. Our study is motivated by the alluring prospect of engineering spin-spin interactions in nanodevices with specific functionality at the surface of metals. In particular, the choice of Pb was motivated by its importance in experiments where superconductivity and strong spin-orbit Rashba interactions (which emerge due to the lack of inversion symmetry at the surface) are combined. We have been able to estimate the Rashba parameter as $\alpha_R \approx 0.97$ eV Å.

In this work, assuming classical impurity spins $\mathbf{S}_1$ and $\mathbf{S}_2$ weakly coupled to the Pb substrate via a generic *s-d* model (a situation that corresponds to a large class of experimental systems), we have developed a method which combines realistic *ab initio* calculations with low-cost computational effort. Using second-order perturbation theory and realistic DFT calculations for the electronic band structure of clean Pb(110), we have been able to systematically obtain the effective spin Hamiltonian between $\mathbf{S}_1$ and $\mathbf{S}_2$ at order J_{sd}^2 with no additional assumptions. Since our method is perturbative, the underlying electronic structure of clean Pb(110) obtained within *ab initio* is not modified. Technically, this means that the method, which is suitable for DFT band-structure calculations based on a periodic lattice, involves relatively small unit cells. This fact results in a considerable minimization of computational effort. It is worth mentioning that, in general, the calculation of realistic nanoscale spin interactions through *ab initio* methods involves a great deal of computational effort (see, e.g., Ref. [55]). Our method allows us to systematically track the contribution of the conduction-electron propagators to the magnetic interaction functions [see Eqs. (20)–(22)]. In addition to the well-known RKKY interaction, the presence of Rashba spin-orbit coupling induces finite DM and tensor matrix interactions, proportional to α_R and α_R^2, respectively. In particular the DM interaction is responsible for noncollinear magnetism and chiral effects (see Fig. 5, where we obtain noncollinear configurations from the minimization of the effective Hamiltonian). These types of interactions were recently investigated in relation to Majorana proposals and skyrmion systems, which are currently being investigated for magnetic storage technology.

The philosophy of our work is reminiscent of those of Imamura *et al.* [44], Zhu *et al.* [56], and Bouaziz *et al.* [26], in which generic indirect magnetic interactions are obtained directly from the conduction electrons. However, in contrast to those works we have not assumed any specific model Hamiltonian for the conduction electrons. In that sense, this represents an important improvement since it allows us to use the knowledge of realistic band-structure calculations. We point out that in many cases where Rashba spin-orbit coupling is present, there is a tendency to use phenomenological two-dimensional (2D) conduction band models [26,44]. However, it is known that bulk electrons cannot be neglected and that they play an important role in systems of adatoms on metallic surfaces [57–59]. A consequence of neglecting bulk electrons is the unrealistic slow decay of the RKKY and other indirect exchange interactions. In addition, in certain cases it has been identified that the presence of Van Hove singularities in the idealized 2D band structure produces anomalous long-range interactions [26].

Being a perturbative approach based on the second-order expansion (i.e., the "RKKY approximation"), our method does not take into account higher-order scattering terms, and therefore, it is intrinsically limited to the weak-coupling regime $\rho_{3D} J_{sd} \ll 1$. In that respect, we briefly mention that extensions to include higher-order scattering terms have been proposed in the past [26,55,60]. However, in the case of impurities in the strong-coupling Kondo regime, even including higher-order scattering terms might not be enough due to the breakdown of the perturbative expansion. In that case, many-body effects such as Kondo correlations, mixed-valence behavior, charge excitations, etc., should be addressed from the beginning for a proper description. In fact, one of the most severe limitations of the perturbative method is its failure to describe the competition between the RKKY interaction and the Kondo effect. In that respect, Allerdt *et al.* [61,62], Mitchell *et al.* [63], and Schwabe *et al.* [64] recently considered many-body nonperturbative effects of the *s-d* exchange on the interaction between quantum impurities at the surface of metals by implementing the density-matrix renormalization group or the numerical renormalization group. While the method described in this work is certainly not applicable to such situations, we stress that numerous experimental realizations of adatoms on top of metallic surfaces never reach the strong-coupling Kondo limit, and therefore, the perturbative approach can be safely applied. Such is the case when the temperature is $T > T_K$ or when the external magnetic fields are

$B > k_B T_K/\mu_B$, with T_K being the Kondo temperature. In those cases, the crossover to the strong-coupling limit is interrupted by the energy scales associated with T and B, respectively. In addition, it is usually the case that impurities deposited on metallic surfaces exhibit a large spin value together with large single-ion anisotropy terms [such as $D(S^z)^2$], effects which tend to quench quantum fluctuations and the Kondo effect, making it possible to treat the impurities as classical objects. In particular, the Appelbaum-Anderson perturbative approach [52–54] was successfully applied by Zhang *et al.* [41], showing remarkable agreement with experiment.

Another important conclusion of our work is the strong anisotropy of the induced interactions depending on the directionality (a or b direction in Figs. 3 and 4) as a result of the symmetry of the Pb(110) surface. This result was also obtained theoretically [55] and experimentally [12] in different systems. In addition, the interaction is nonmonotonic with the distance. These two aspects are in stark contrast with respect to the usually idealized parabolic-band RKKY.

Finally, we note that the band structure of Pb has been computed for the normal state and that the superconducting gap in the spectrum of quasiparticle excitations of Pb has been ignored. We speculate that this approximation will not affect our results, as the superconducting effects should appear at distances of the order of the coherence length $\xi_{\mathrm{Pb}} \approx 80$ nm, which are much larger than the interatomic distances in our calculations.

In summary, by combining *ab initio* methods with perturbation theory, we have studied the realistic indirect spin-spin interactions mediated by conduction electrons in the metallic surface of Pb(110). We speculate that this approach might be helpful in the design of weakly coupled magnetic nanostructures with tailored interactions in order to obtain specific functionalities.

ACKNOWLEDGMENTS

The authors acknowledge financial support from PICT 2017-2081 (ANPCyT-Argentina). A.M.L. acknowledges financial support from PIP 11220150100364 (CONICET-Argentina) and Relocation Grant No. RD1158-52368 (CONICET-Argentina).

[1] M. A. Ruderman and C. Kittel, Phys. Rev. **96**, 99 (1954).
[2] T. Kasuya, Prog. Theor. Phys. **16**, 45 (1956).
[3] K. Yosida, Phys. Rev. **106**, 893 (1957).
[4] M. N. Baibich, J. M. Broto, A. Fert, F. Nguyen Van Dau, F. Petroff, P. Etienne, G. Creuzet, A. Friederich, and J. Chazelas, Phys. Rev. Lett. **61**, 2472 (1988).
[5] S. Doniach, Phys. B (Amsterdam, Neth.) **91**, 231 (1977).
[6] A. C. Hewson, *The Kondo Problem to Heavy Fermions* (Cambridge University Press, New York, 1993).
[7] H. v. Löhneysen, A. Rosch, M. Vojta, and P. Wölfle, Rev. Mod. Phys. **79**, 1015 (2007).
[8] E. Z. Meilikhov, Phys. Rev. B **75**, 045204 (2007).
[9] Wang Dan and Xiong Shi-Jie, Chin. Phys. Lett. **25**, 1102 (2008).
[10] P. Wahl, P. Simon, L. Diekhöner, V. S. Stepanyuk, P. Bruno, M. A. Schneider, and K. Kern, Phys. Rev. Lett. **98**, 056601 (2007).
[11] F. Meier, L. Zhou, J. Wiebe, and R. Wiesendanger, Science **320**, 82 (2008).
[12] L. Zhou, J. Wiebe, S. Lounis, E. Vedmedenko, F. Meier, S. Blügel, P. H. Dederichs, and R. Wiesendanger, Nat. Phys. **6**, 187 (2010).
[13] A. A. Khajetoorians, J. Wiebe, B. Chilian, S. Lounis, S. Blügel, and R. Wiesendanger, Nat. Phys. **8**, 497 (2012).
[14] A. A. Khajetoorians, M. Steinbrecher, M. Ternes, M. Bouhassoune, M. dos Santos Dias, S. Lounis, J. Wiebe, and R. Wiesendanger, Nat. Commun. **7**, 10620 (2016).
[15] T. Esat, B. Lechtenberg, T. Deilmann, C. Wagner, P. Krüger, R. Temirov, M. Rohlfing, F. B. Anders, and F. S. Tautz, Nat. Phys. **12**, 867 (2016).
[16] S. Nadj-Perge, I. K. Drozdov, B. A. Bernevig, and A. Yazdani, Phys. Rev. B **88**, 020407(R) (2013).
[17] J. Klinovaja, P. Stano, A. Yazdani, and D. Loss, Phys. Rev. Lett. **111**, 186805 (2013).
[18] B. Braunecker and P. Simon, Phys. Rev. Lett. **111**, 147202 (2013).
[19] S. Nadj-Perge, I. K. Drozdov, J. Li, H. Chen, S. Jeon, J. Seo, A. H. MacDonald, B. A. Bernevig, and A. Yazdani, Science **346**, 602 (2014).
[20] M. Ruby, F. Pientka, Y. Peng, F. von Oppen, B. W. Heinrich, and K. J. Franke, Phys. Rev. Lett. **115**, 197204 (2015).
[21] R. Pawlak, M. Kisiel, J. Klinovaja, T. Meier, S. Kawai, T. Glatzel, D. Loss, and E. Meyer, npj Quantum Inf. **2**, 16035 (2016).
[22] B. E. Feldman, M. T. Randeria, J. Li, S. Jeon, Y. Xie, Z. Wang, I. K. Drozdov, B. Andrei Bernevig, and A. Yazdani, Nat. Phys. **13**, 286 (2016).
[23] N. Tsukahara, S. Shiraki, S. Itou, N. Ohta, N. Takagi, and M. Kawai, Phys. Rev. Lett. **106**, 187201 (2011).
[24] T. Komeda, Surf. Sci. **630**, 343 (2014).
[25] J. Girovsky, J. Nowakowski, M. E. Ali, M. Baljozovic, H. R. Rossmann, T. Nijs, E. A. Aeby, S. Nowakowska, D. Siewert, G. Srivastava, C. Wäckerlin, J. Dreiser, S. Decurtins, S.-X. Liu, P. M. Oppeneer, T. A. Jung, and N. Ballav, Nat. Commun. **8**, 15388 (2017).
[26] J. Bouaziz, M. dos Santos Dias, A. Ziane, M. Benakki, S. Blügel, and S. Lounis, New J. Phys. **19**, 023010 (2017).
[27] J. Linder and K. Halterman, Phys. Rev. B **90**, 104502 (2014).
[28] J. Linder and J. W. A. Robinson, Nat. Phys. **11**, 307 (2015).
[29] O. Krupin, G. Bihlmayer, K. Starke, S. Gorovikov, J. E. Prieto, K. Döbrich, S. Blügel, and G. Kaindl, Phys. Rev. B **71**, 201403(R) (2005).
[30] P. Chuang, S.-C. Ho, L. W. Smith, F. Sfigakis, M. Pepper, C.-H. Chen, J.-C. Fan, J. P. Griffiths, I. Farrer, H. E. Beere, G. A. C. Jones, D. A. Ritchie, and T.-M. Chen, Nat. Nanotechnol. **10**, 35 (2014).
[31] S. Bandyopadhyay and M. Cahay, Appl. Phys. Lett. **85**, 1814 (2004).
[32] S. J. Frisken and D. J. Miller, Phys. Rev. Lett. **57**, 2971 (1986).
[33] A. S. Oja, X. W. Wang, and B. N. Harmon, Phys. Rev. B **39**, 4009 (1989).

[34] R. C. Patnaik, R. L. Hota, and G. S. Tripathi, Phys. Rev. B **58**, 3924 (1998).
[35] B. Harmon, X.-W. Wang, and P.-A. Lindgård, J. Magn. Magn. Mater. **104–107**, 2113 (1992).
[36] P. Kim and J. H. Han, Phys. Rev. B **87**, 205119 (2013).
[37] A. Kundu and S. Zhang, Phys. Rev. B **92**, 094434 (2015).
[38] T. Kikuchi, T. Koretsune, R. Arita, and G. Tatara, Phys. Rev. Lett. **116**, 247201 (2016).
[39] K. J. Franke, G. Schulze, and J. I. Pascual, Science **332**, 940 (2011).
[40] B. W. Heinrich, L. Braun, J. I. Pascual, and K. J. Franke, Nano Lett. **15**, 4024 (2015).
[41] Y.-h. Zhang, S. Kahle, T. Herden, C. Stroh, M. Mayor, U. Schlickum, M. Ternes, P. Wahl, and K. Kern, Nat. Commun. **4**, 2110 (2013).
[42] J. W. Negele and H. Orland, *Quantum Many Particle Systems* (Addison-Wesley, Reading, MA, 1987).
[43] G. D. Mahan, *Many Particle Physics* (Plenum, New York, 1981).
[44] H. Imamura, P. Bruno, and Y. Utsumi, Phys. Rev. B **69**, 121303(R) (2004).
[45] G. Kresse and J. Hafner, Phys. Rev. B **47**, 558 (1993).
[46] G. Kresse and J. Furthmüllerb, Comput. Mater. Sci. **6**, 15 (1996).
[47] G. Kresse and J. Furthmüller, Phys. Rev. B **54**, 11169 (1996).
[48] H. J. Monkhorst and J. D. Pack, Phys. Rev. B **13**, 5188 (1976).
[49] G. Kresse and D. Joubert, Phys. Rev. B **59**, 1758 (1999).
[50] G. I. Csonka, J. P. Perdew, A. Ruzsinszky, P. H. T. Philipsen, S. Lebègue, J. Paier, O. A. Vydrov, and J. G. Ángyán, Phys. Rev. B **79**, 155107 (2009).
[51] K. Würde, A. Mazur, and J. Pollmann, Phys. Rev. B **49**, 7679 (1994).
[52] J. Appelbaum, Phys. Rev. Lett. **17**, 91 (1966).
[53] P. W. Anderson, Phys. Rev. Lett. **17**, 95 (1966).
[54] J. A. Appelbaum, Phys. Rev. **154**, 633 (1967).
[55] H. Ebert and S. Mankovsky, Phys. Rev. B **79**, 045209 (2009).
[56] J.-J. Zhu, D.-X. Yao, S.-C. Zhang, and K. Chang, Phys. Rev. Lett. **106**, 097201 (2011).
[57] N. Knorr, M. A. Schneider, L. Diekhoner, P. Wahl, and K. Kern, Phys. Rev. Lett. **88**, 096804 (2002).
[58] M. A. Schneider, L. Vitali, N. Knorr, and K. Kern, Phys. Rev. B **65**, 121406(R) (2002).
[59] L. Limot and R. Berndt, Proceedings of the Seventh International Symposium on Atomically Controlled Surfaces, Interfaces and Nanostructures, special issue of Appl. Surf. Sci. **237**, 572 (2004).
[60] P. Lloyd and P. Smith, Adv. Phys. **21**, 69 (1972).
[61] A. Allerdt, C. A. Büsser, G. B. Martins, and A. E. Feiguin, Phys. Rev. B **91**, 085101 (2015).
[62] A. Allerdt, R. Žitko, and A. E. Feiguin, Phys. Rev. B **95**, 235416 (2017).
[63] A. K. Mitchell, P. G. Derry, and D. E. Logan, Phys. Rev. B **91**, 235127 (2015).
[64] A. Schwabe, M. Hänsel, M. Potthoff, and A. K. Mitchell, Phys. Rev. B **92**, 155104 (2015).